Deep Ocean Energy Harvesting

Point Absorber Design

Jasmine Feliciano, Nick Hernandez, Yao Long, and Julia White

With the Assistance of Professor Robert Daniello

4/25/2018

Abstract

In a world where fossil fuels are being steadily depleted, new energy sources are being sought out. Ocean energy is a renewable resource that has yet to be fully utilized. Waves are a consistently available resource, in spite of weather changes or time of day. Wave energy has the potential to supply power for a variety of applications ranging from supplying the grid to remote applications such as marine research and ocean reconnaissance. The goal of this project was to use a point absorber style wave energy converter to harvest the kinetic energy of waves. We designed and built a 1:15 scale model to test the mooring capabilities and power output. In order to calculate the power output, we measured the pressure output and stroke length, which could then be scaled to estimate a full-size wave energy converter.

Table of Contents

1. Introduction

The global demand for energy has increased significantly in recent years, depleting the world's supply of nonrenewable resources such as oil, gas, and coal. These types of resources generate approximately 80 percent of the world's energy, with only 20 percent coming from renewable resources such as solar, wind, and waves (Energy smart, n.d.) This proves to be a great concern, as the search for efficient alternative energy systems is becoming more urgent.

For ocean-based operations, waves are readily available throughout the day and do not heavily fluctuate. Waves consist of higher energy density flow five times more dense than wind energy, and 20 to 30 times more dense than solar (Amir, Sharip, Muzanni, & Anuar, 2016). This makes it a viable form of renewable energy for ocean-based applications. Through the development of a portable wave energy converter (WEC), devices like autonomous underwater vehicles (AUVs) have the potential to explore further ranges and perform more power-intensive operations. The main AUV users are the Navy and large ocean research groups, both of whom could benefit from a heavier reliance on wave energy. The portable device can be stored on a ship, allowing it to be easily transported to the site of the AUV operation. This alleviates the common issue of towing the AUV back to shore for charging.

There are several types of WECs on the market, ranging from overtopping devices to point absorbers. This project focused on a point absorber design due to its size. Of all devices currently used, it creates the most energy for the smallest mass. These devices can be floating, meaning they could be used for deep ocean applications. These devices convert the kinetic energy of waves by oscillating a piston vertically, which then drives a generator to create electrical energy (Voorhis, 2012).

Testing was conducted in WPI's Sports and Recreation Center pool to measure the pressure output and stroke length of the prototype, which could be scaled to estimate a full-size WEC. Additionally, a small scale test was proposed to better understand wave characteristics, as well as to determine the relationship between force and spring stiffness of the system.

2. Literature Review

2.1 Wave Energy

The ocean is normally associated with marine life, recreational activities, and transportation; however, the power contained within waves is often disregarded due to the fact that WECs are underdeveloped in comparison to other forms of alternative energies (Duggan, 2016; Ocean Energy Council, 2017). An average coastal wave gives off 35,000 horsepower per mile of coast. This energy could be used to power a variety of industrial and residential operations. In fact, one coastal wave is enough to power two average U.S. homes in one month (Ocean Energy Council, 2017).

A wave's power generation draws back to its formation. Waves are created constantly, formed by strong winds and the rotation of the Earth. In the open ocean, these winds create a series of chaotic waves, leading to a regular sequence of swells. As these swells approach the coast, the wavelengths shorten, the height of the waves increase, and the waves break on shore (Tester, 2012).

There is great potential in harvesting wave energy because waves are abundant, readily available at all times, and have the potential to provide a vast amount of power. When compared to the annual world energy consumption of 148,000 TWh in 2008 (Richter, Magana, Sawodny, & Brekken, 2013), the oceans could potentially provide 10 – 20% of the Earth's energy (Future Marine Energy, n.d.). This shows the potential impact of wave energy on the future of the renewable industry.

2.2 Wave Energy Converters

There are numerous types of existing WECs that attempt to harness either the potential or kinetic energy of waves to convert it into electricity. Many of these WECs vary in size, shape, functionality, and energy output; however, they can be divided up into four main categories: oscillating water columns, overtopping devices, attenuators, and point absorbers, seen in Figures 2.2.1-2.2.4. Each of these WECs have their own distinguishable attributes along with advantages and disadvantages.

Oscillating water columns, seen in Figure 2.2.1, are normally constructed along the shoreline to capture energy from crashing waves. These columns function due to the pressure differential created between air and the ocean within a partially submerged structure. The pressure from the waves pushes air through a hollow chamber attached to a turbine. A decrease in water pressure then pulls the air back through the turbine, generating electricity (Kempener & Neumann, 2014). The main advantage of these systems are that they are robust and fairly simple due to the utilization of only one moving part: the air turbine (Mathew, 2013). This also allows oscillating water columns to convert energy at low maintenance costs with a conversion efficiency of around 75% (Mathew, 2013; Nader, 2013). Although the cost of harnessing the energy can be minimized, there are some areas of concern. These structures operate exclusively on the shoreline, meaning they have no portability. Oscillating water columns may also pose a threat to many marine habitats along the coast (Mathew, 2013).
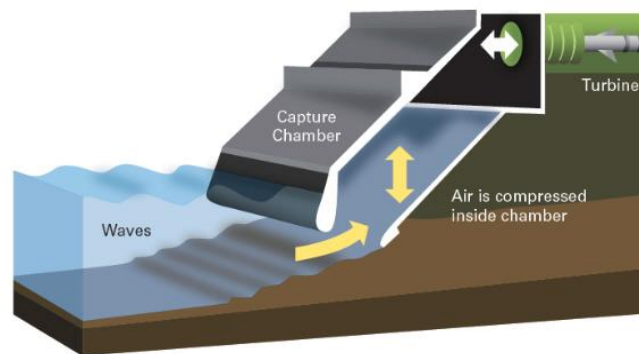

Figure 2.2.1 Oscillating Water Column (Mathew, 2013)

Overtopping devices consist of a ramp leading up to an artificial reservoir with a retaining wall. Similar to an oscillating water column, this device operates based on the pressure differential created between the reservoir and the surrounding ocean. The potential energy, due to the height of collected water, is then converted to power through turbines located below the reservoir, shown in the Figure 2.2.2. As the water level rises, waves crash over the ram, creating a pressure gradient. This results in water being forced out through the turbines within the device. Unlike oscillating water columns, these structures can yield much greater amounts of power due to their ability to capture a large volume of waves and generate electricity without the use of internal mechanisms. This also minimizes costs for maintenance and repair (Tethys, n.d.). Overall, these devices typically range in efficiency from 70-80% (Poullikkas, 2014). Despite these advantages,

3

overtopping devices lack portability. Additionally, due to their large size, they can be a hazard for sea life in the ocean due to the possibility of fish getting trapped inside the reservoirs (Tethys, n.d.).
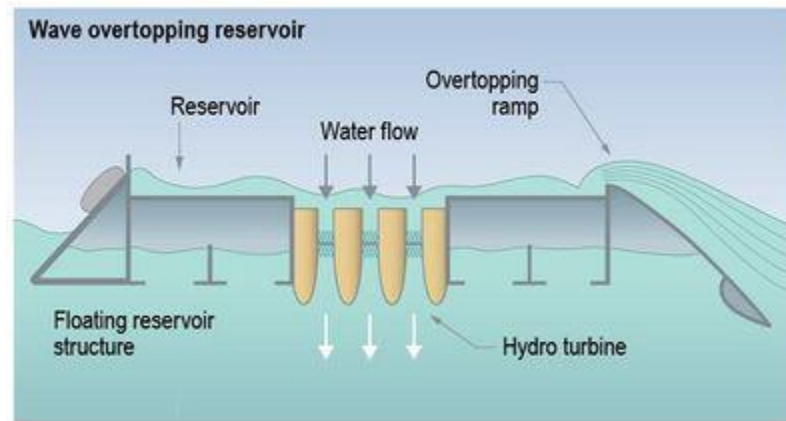

Figure 2.2.2 Overtopping Device (Wave and ocean thermal energy devices, n.d.)

Surface attenuators are long, cylindrical structures with multiple floating segments that are oriented perpendicular to incoming waves, which can be seen below in Figure 2.2.3. These segmented regions allow the device to bob in the water, which then drives hydraulic pumps to generate electricity. Attenuators are able to capture a wide range of waves due to their large size, thus providing a large power output with a conversion efficiency of 40% (University of Strathclyde, 2017) They are also very sturdy and can withstand harsh environments. The environmental concerns are similar to those of both the overtopping devices and oscillating water columns where marine life may possibly get trapped or entangled within the joints of the system (Tethys n.d.).

Figure 2.2.3 Surface Attenuator (Ocean wave energy, 2017)

Lastly, point absorbers are buoy-like systems that float on the surface of the water. The motion of waves causes the device to bob up and down, which in turn generates electricity. Point absorbers depend on an internal power take-off (PTO) system that pumps air to power the generator as the cylinder is compressed and released. They rely on a constant supply of waves and can attain maximum efficiency by matching the optimal frequency and wave height (Voorhis, 2012). These devices have the potential to provide a large amount of power in a relatively small system, making them ideal for portable usage. They are also a versatile technology due to their ability to harvest energy from waves coming in all directions and can be operational for long durations of time (Kalofotias Fillipos, 2016). Some disadvantages of point absorbers include their struggle to adapt to the varying heights and frequencies of waves and the threat posed onto the system by major storms, which can also greatly reduce their efficiency. An example of a point absorber can be seen in Figure 2.2.4.
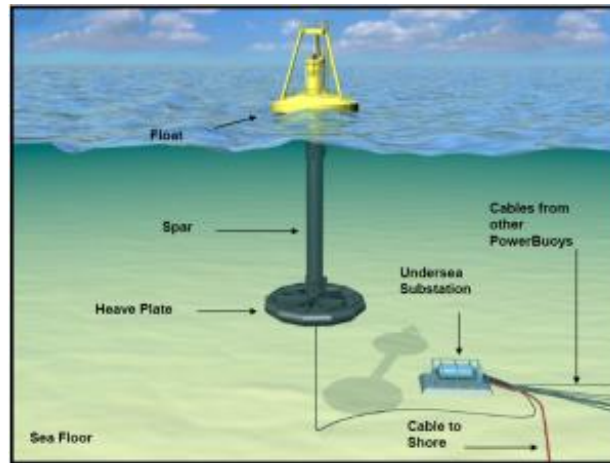
Figure 2.2.4 Point Absorber (Ocean Power Technologies, 2017)

This point absorber is a PowerBuoy, designed by Ocean Power Technologies, a company based in New Jersey. Ocean Power Technologies plans to launch a series of these WECs in the Southern Ocean, off the coast of Victoria, Australia to generate up to 10 megawatts of electricity (Hawaii Department of Business, 2002). There are several models of PowerBuoys that have been designed for different power ratings; the PB-3 with a 3 kW rating, the PB-15 with a 15 kW rating, and the PB-40 with a 40 kW power rating (Ocean Power Technologies, 2017). The conversion efficiency of the PB-3 is reported to be between 30-45% (Ocean Power Technologies, 2011). The conversion efficiency of the PB-3 is reported to be between 30-45% (Ocean Power Technologies, 2011). PowerBuoys are one of hundreds of WECs that have been suggested for research and implementation.

2.3 Power Take Off Systems

One of the leading components in determining the overall efficiency of WECs is the power take off system (Têtu, 2017). This component operates by transforming energy absorbed by the primary converter into electricity (Têtu, 2017). In addition to impacting overall efficiency, the system is important from an economic standpoint, as it accounts for 20-30% of the initial investment for a WEC (Têtu, 2017). Due to the impact on system performance and financial investment, time should be spent analyzing PTO systems to determine which system will meet both efficiency and energy conversion needs.

Hydraulic converters are a type of PTO that translate kinetic energy from the system into electricity (Têtu, 2017). The device itself is considered simple with low investment, operation, and

maintenance costs (du Plessis, 2012). In addition, the system has been shown to have efficiencies of 71-76%, and fares well in rough waters (Ulvin, Molinas, & Sjolte, 2012). While the system seems to be highly practical, it does have some design challenges.
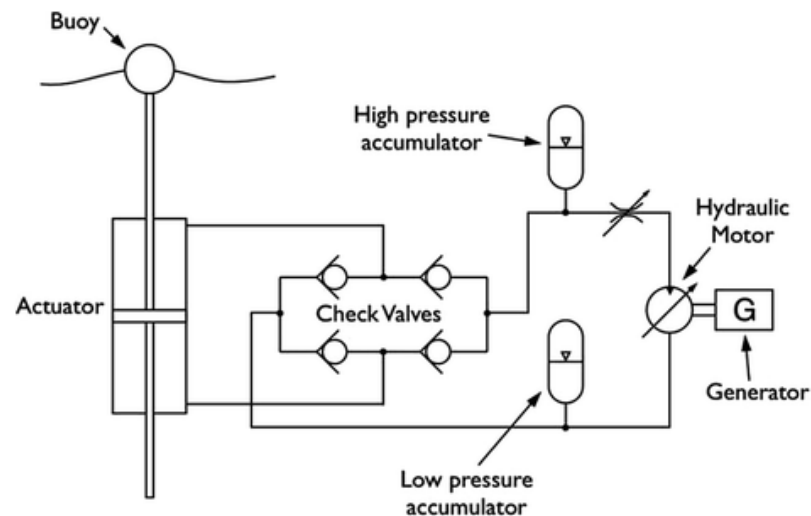

Figure 2.3.5: Hydraulic Power Take Off System in a Point Absorber (Têtu, 2016, pg. 211)

Point absorbers utilize a hydraulic power take off system, a schematic of which can be seen in Figure 2.3.5. The buoy on the point absorber is attached to an actuator. The oscillating motion of the buoy is translated to the actuator, thereby pushing fluid into the hydraulic motor through the check valves. This motor then powers the generator, producing electricity. The high and low pressure accumulators are in the system in order to regulate fluid flow (Têtu, 2016, pg. 211). This system is used because it translates oscillating motion to electricity.

Hydro turbines are PTOs that convert potential energy into electricity (Têtu, 2017). The system requires low maintenance and can achieve efficiencies in excess of 90% (Têtu, 2017). The hydro turbine itself was designed to be the only moving part within the WEC, decreasing the need for overall system maintenance as well as lifetime costs (Simple and robust construction - complex design, 2005). This also minimizes disruption to marine life and damage from debris collisions (Simple and robust construction - complex design, 2005). Hydro turbines were specifically designed to benefit overtopping devices (Simple and robust construction - complex design, 2005), making the system specialized, and as a result, not widely applicable.

For a PTO to achieve functionality, it needs to utilize a control system. The most simplistic system is known as passive loading control, which uses counter-balancing techniques to limit unwanted system movement (Têtu, 2017). This limitation serves as protection against damage in extreme motion and works through sensing angular velocity and providing a set counter torque

7

(Têtu, 2017). This control system also levels out the power harvested by the WEC for a smaller peak to mean power ratio (Wang & Isberg, 2015). The simplicity of the system provides a cost effective option that allows electro-mechanical limitations to be respected through only targeting control of the amplitude of oscillation (Ulvin et al., 2012). Passive loading works through control of device damping and limits the maximum power extracted when faced with large waves (Ulvin et al., 2012). These large waves are the type typically encountered in the deep ocean, where AUVs would be travelling. However, the simplicity of the passive loading control limits its effectiveness. When facing large waves, the system extracts limited power due to high resistance output (Ulvin et al., 2012).

Reactive loading control works through actively adjusting the spring coefficient, inertia, and oscillator damping of the WEC in order to maximize the energy absorption at all wave frequencies (Hong et al., 2014; Têtu, 2017). This creates a more complex system that in turn is more adaptive. Reactive loading, like passive loading, adapts to higher waves to prevent system damage, limiting energy harvested from waves with large amplitudes (Ulvin et al., 2012). One drawback to this system is that it can produce negative current when bobbing downwards (Wang & Isberg, 2015).

PTOs generate power through harnessing the motion of wave energy. However, waves characteristics are not constant or entirely predictable, therefore making the process inconsistent. This unsteadiness is often combated by implementing an energy storage system.

2.4 Energy Storage

The main energy storage technique currently employed is batteries due to their high energy density, proven effectiveness, and low standby losses (Chen et al., 2009; Raghunathan, Kansal, Hsu, Friedman, & Srivastava, 2005). Batteries are often the preferred method because they respond quickly to load changes, making them useful for unsteady power generation, such as the case of renewable energy (Chen et al., 2009). Oftentimes, systems are designed around a battery, with four main types including nickel cadmium, nickel metal hydride, lithium ion, and sealed lead acid (Raghunathan et al., 2005).

Lead acid and nickel metal hydride both have poor low temperature performance and therefore require external heating systems (Chen et al., 2009). Lead acid is the oldest and therefore most proven battery, however it has low energy density and high weight (Raghunathan et al.,

2005). These batteries typically have a life cycle of 500-1000 cycles and an efficiency of 70-90% (Chen et al., 2009). Nickel metal hydride batteries typically achieve 500 cycles before dropping down to 80% efficiency, showing a longer life than lead acid (Raghunathan et al., 2005). For deep ocean waters, where temperatures can range 12-20°C (Bergman, 2011), these batteries are not practical for ocean applications.

Lithium ion and nickel cadmium both operate well at low temperatures (BU-407: Charging nickel-cadmium, n.d.). Lithium ion is the most expensive battery available, however it is also the most efficient with an efficiency of almost 100% (Chen et al., 2009; Raghunathan et al., 2005). Lithium batteries also experience a long lifespan of 10,000 cycles (Chen et al., 2009). Nickel cadmium batteries, however, have been around for around 100 years, showing a proven reliability and many opportunities for development (Chen et al., 2009). These batteries are low maintenance, although they have shown capacity loss (Chen et al., 2009; Raghunathan et al., 2005). To compare these two batteries, Table 2.4.1 has been provided below.

Battery Type	Energy Density	Lifecycle	Efficiency	Discharge Temperature
Nickel Cadmium	50-75 Wh/kg[1]	2,000-2,500[1]	91%[2]	-20 to 65°C[2]
Lithium Ion	200 Wh/kg[1]	10,000[1]	~100%[1]	-20 to 60°C[2]

Table 2.4.1 Nickel Cadmium and Lithium Ion Battery Comparison

1(Chen et al., 2009)

2(BU-407: Charging nickel-cadmium.)

Due to the portability and size of batteries, they are seen as the top option to store energy from many renewable sources, such as wind turbines and solar panels. However, batteries extend beyond this storage. They are also used to power many vehicles, such as AUVs.

2.5 Autonomous Underwater Vehicles

Autonomous underwater vehicles are becoming a widely used option in the defense and marine research industries. AUVs are underwater vehicles that are programmed by an operator to perform a specific function (Crimmins & Manley, 2008). AUVs provide a wide range of utility

achieved from their various sizes, ranging from a small, portable device under 100 pounds to a large vehicle weighing several thousand pounds. AUVs are becoming more appealing to large-scale marine applications due to rising fuel costs (Wynn et al., 2014). All AUVs carry a power source onboard in order to provide energy to propellers, thrusters, and other equipment needed to perform operation.

AUVs provide a wide variety of applications for the defense industry. Since the 1990s, the Office of Naval Research has invested in the development of AUV technology for military purposes such as underwater mine hunting (Hydroid, n.d.). The use of AUVs for undersea mine detection not only provides cost savings when compared to the costs of operating a ship and personnel, but also eliminates the risk for human divers. Aside from mine detection, the Navy has identified 8 other capabilities that AUVs provide for naval operation: intelligence, surveillance, and reconnaissance (ISR); anti-submarine warfare; inspection; oceanography; communication; payload delivery; information operations; and time critical strike (U.S. Department of the Navy, 2004).

In addition to the defense industry, AUVs have made great contributions to marine studies, including the mapping of the seafloor and water columns, along with hydrothermal vent studies. The Lost City hydrothermal vent field was mapped by ABE, an AUV. Another AUV, SENTRY, explored the hydrothermal venting on the Galapagos Rift (Bradley, Feezor, Singh, & Sorrell, 2001). AUVs can operate in depths of 6000 m and move at speeds of 1.5 - 2.0 m/s, depending on extreme environments and tidal currents.

The REMUS 6000 uses up to two 12 kWh rechargeable Li-ion batteries, while the REMUS 600 uses up to two 5.4 kWh rechargeable Li-ion batteries. Other AUVs such as the MAYA AUV uses lithium polymer cells for about 7.2 hours. Depending on AUV size, bus voltages range from 6V to 48V batteries (Bradley et al., 2001). The Odyssey and ABE are 2 - 3 m in length and use a 48V battery. It's common for AUVs to use specialized batteries to power the system, but fuel cells and solar energy have also been investigated for powering AUVs (Crimmins & Manley, 2008).

2.5 Conclusion

Wave energy is an actively evolving field. As it expands, there are several opportunities for innovation and improvement. Both the kinetic and potential energies contained within a wave can be extracted coastally or out in deep waters, making the practice highly versatile. Ocean based

organizations and communities such as the Navy may utilize WECs for the development of their green energy goals. A system utilizing a combination of energy harvesting tactics may therefore be the most effective option for power extraction.

3. Methodology

3.1 Overview of Goals

In order to create a usable system, a set of specifications were set forth based on the design of Ocean Power Technologies' PB-3 model. These specifications were determined by factors ranging from material properties to size constraints. The project mainly focused on designing a point absorber to create a more efficient, renewable energy based system for charging AUVs.

In order for the WEC to sufficiently provide power to charge AUVs, the system must meet several energy requirements. To service a range of AUVs, the proposed system will store 12 kWh. This energy storage requirement was set forth based on the research performed on pre-existing AUVs such as the REMUS 6000 and the MBARI Dorado. These AUVs are larger vessels that are capable of exploring depths of up to 6000 meters, therefore the energy storage requirements were based on the power requirements of the REMUS 6000.

Once the 12 kWh requirement was set forth, Ocean Power Technologies' PB-3 WEC was identified to be able to produce the energy required. The dimensions for the PB-3 can be found in Table 3.1.1. This observation provided an estimate of the size needed for a full-scale WEC. Additionally, the dimensions of the REMUS 6000 were considered in the design of the WEC to accommodate for a battery charging station. The system design was intended to be easily transported and deployed such that it can be moved to a location where an AUV is operating.

Ocean Technologies PB-3 Dimensions	
Height (m)	14.3
Spar Diameter (m)	1
Float Diameter (m)	2.7

Table 3.1.1 Ocean Technologies PB-3 Dimensions (Ocean Power Technologies, 2017)

Mooring will ensure that the WEC does not move with the waves by providing a resistance so that energy can be successfully harvested while still allowing the system to oscillate vertically. The PB-3 utilizes a heave plate at the bottom of the spar as its mooring system, but anchors are also used in other mooring systems. For our system, we chose to forego an anchor to allow deep ocean charging of AUVs.

3.2 Simulation of Full Scale Model

During the first 6 months of the project, several variations of the design for a full scale device were created through sketching and SolidWorks modeling. We designed the major components based off of the 8 kWh PowerBuoy by Ocean Power Technologies. Using pre-existing designs, we followed a model similar to Figure 3.2.1.
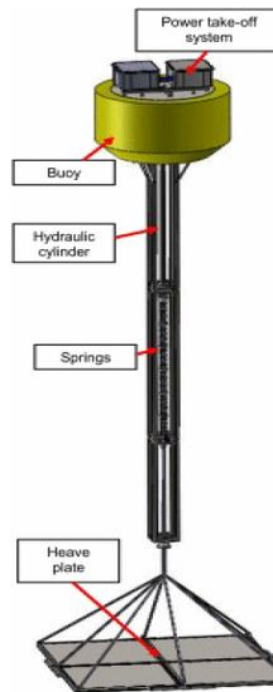

Figure 3.2.1 PB-3 (Engin & Yeşildirek, November 2015)

Though, because of monetary limitations and resource restrictions, we simplified our design to meet our testing requirements and designed a 1:15 scale model. This first SolidWorks iteration, seen in Figure 3.2.2, consists of the heave plate, spar, and bouy. The PTO and electronics were not modeled for the purposes of this project.
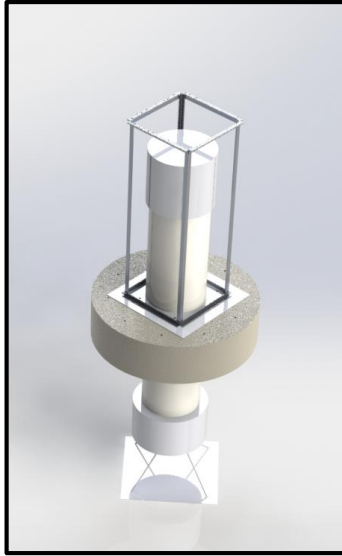
Figure 3.2.2 SolidWorks Model first Render

With the budget and time allocated for building and testing, a simplified prototype was constructed. Creating the entire system following the first iteration would be out of budget and would take longer than the time span of this project. For simplicity, the prototype consisted of off-the-shelf parts including a copper float, a polycarbonate pipe, a pneumatic cylinder to act as a piston, an acrylic heave plate, and air as the working fluid.

3.3 Prototyping Procedure

To effectively prototype the model, we first determined what we wanted to measure from our prototype. The measurements desired were stroke length of the piston and the force that the piston exerts as a response to the buoy. To measure these, a transparent tube was used to house the piston device.

To simplify the model for testing, we chose a pneumatic cylinder rather than a hydraulic cylinder. To scale the prototype, a feasible wave height was first determined. This was set at 3 in, and the average ocean wave height is about 1 m. This set the scaling factor to 1:15. Table 3.3.1 shows the dimensions subsequently determined for the prototype, based on the dimensions of a PB-3.

	PB-3 (m)	Scaled Model (m)	Inches
Float Diameter	2.7	0.18	7.086618
Spar Diameter	1	0.06666666667	2.624673333
Height	14.3	0.9533333333	37.53282867

Table 3.3.1 Scaled Prototype Dimensions

This scale determined the parts ordered for the prototype. For full information on part specifications, see Appendix A.

The float diameter was rounded up to 8 in. from 7 in. due to availability of parts. The material of the float was copper due to part price and durability in water. The spar diameter was also increased to a 3.5 in. outer diameter with a 3 in. inner diameter in order to house a properly scaled pneumatic cylinder with a diameter of 2.75 in. The pneumatic cylinder was stainless steel in order to withstand any water contact. The spar was cut to the proper height, which was rounded to 37.5 in. The material of the pipe was polycarbonate due to its transparency and price. Finally, the heave plate was chosen as a 12 in. x 12 in. acrylic plate for ease of drilling and additional aluminum stock of 4 in. x 3 in. x 0.75 in. were added to provide enough weight to anchor the system without sinking it to the pool floor.

Additionally, the bottom of the point absorber was designed to be modular such that it would hold more weights as needed. We sealed the top of the device with all-purpose cement in order to minimize any possible leakage.

3.4 Testing Procedure

To test the prototype, a body of water at least 4 feet deep was needed. This would provide the proper depth for vertical oscillation of the buoy, as well as test the effectiveness of using a heave plate for mooring. This area was identified as the WPI Sports and Recreation Center's pool. To create waves, a human subject oscillated two body boards to generate small-scale waves in the pool. These waves ranged from one to two inches in height. Pictures of the prototype in the pool can be seen in Figures 3.4.2 and 3.4.3.

In order to calculate the energy that could be harvested from a wave, the volume and pressure changes within the pneumatic cylinder were taken into account. As the float oscillated up and down from the waves, a GoPro Hero 4 camera was used to capture video of the displacement

of the piston, from which the volume change was calculated. In order to measure the pressure change within the pneumatic cylinder, a differential pressure sensor was utilized. The sensor used to measure the pressure difference was the PX26-005DV, which has a range of ± 5 psid. A circuit consisting of various components was constructed for data collection purposes. A SparkFun RedBoard was used to provide a 5V output and read data from the pressure sensor using the Arduino compiler, and a LM741 operational amplifier was used with a 1 kΩ and 100 kΩ resistor in order to amplify the voltage data from the sensor by 100. A general circuit diagram for collecting data from the differential pressure sensor is shown in Figure 3.4.1.
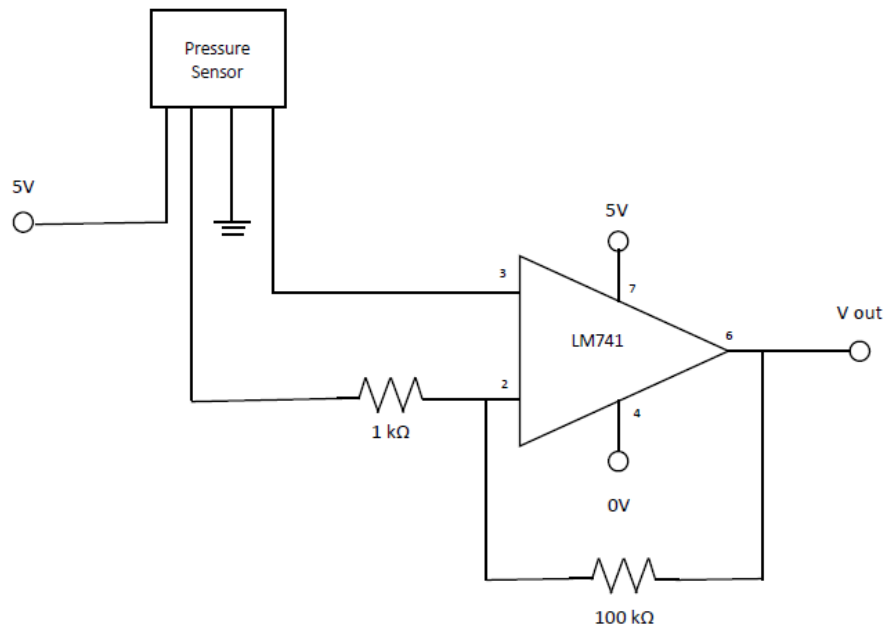

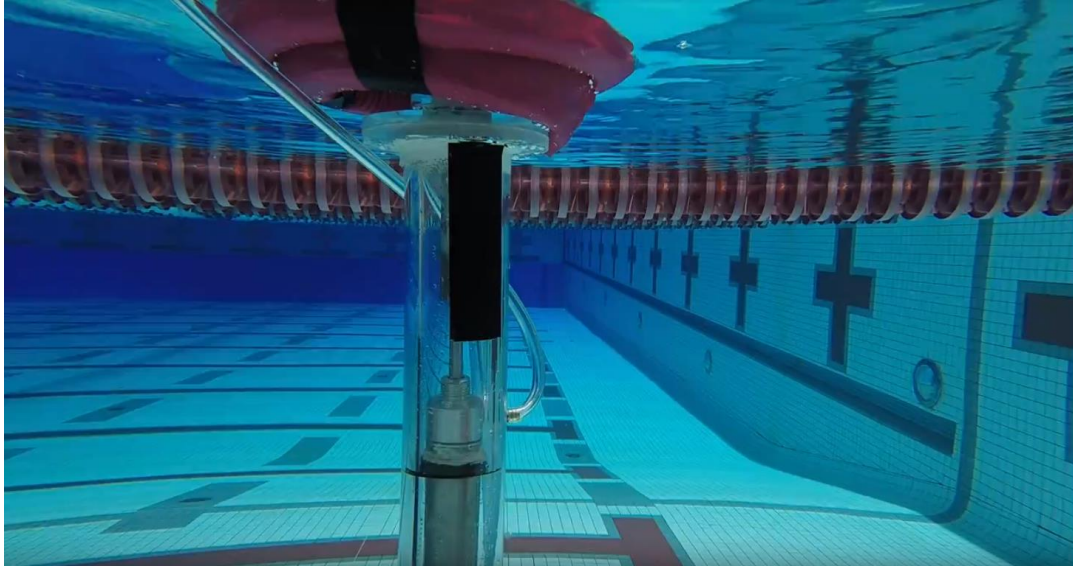*Figure 3.4.1 Circuit Diagram for Experiment*

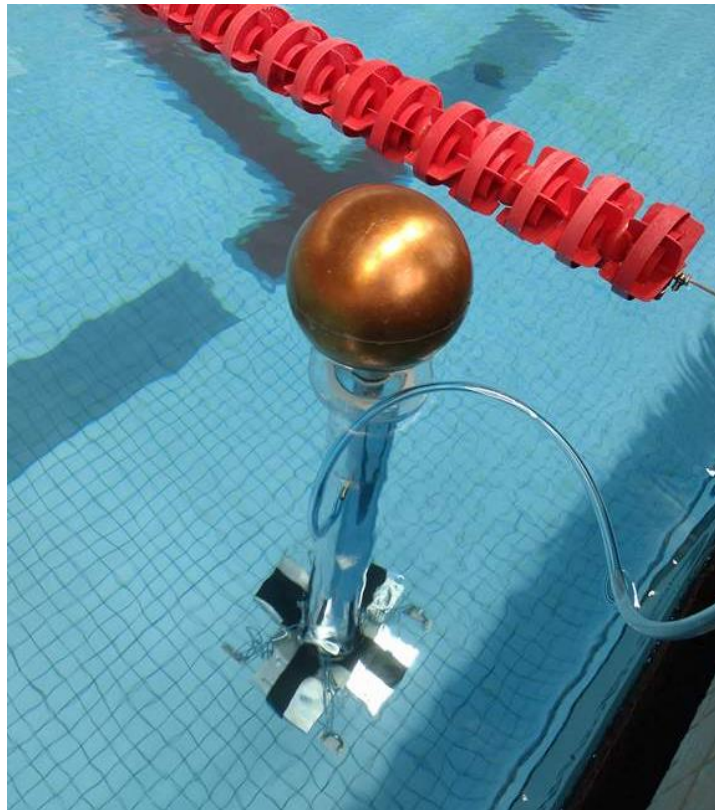*Figure 3.4.2 Underwater View of Prototype in Testing Environment*

Figure 3.4.3 Top View of Prototype in Testing Environment

Additional aquatic floatation devices were attached to the copper float in order to increase ease of upward motion for the buoy. These can be seen attached in Figure 3.4.2. Floatation was increased because the copper float was smaller than ideal, therefore lacking the buoyant force

needed to oscillate the piston. This attachment increased the buoyancy and without any additional suction allowed the piston to more freely oscillate with wave motion. The pressure transducer was connected to the prototype through vinyl tubing, which extended to the poolside where data was being collected off of a laptop. Once the prototype was attached to the pressure transducer with vinyl tubing, additional suction was created, resulting in difficulty with oscillations in conjunction with the small waves being generated. To overcome the suction complications, piston motion was created by pulling on the polycarbonate tube to force oscillations. This resulted in data on pressure output from piston strokes, however it did not generate any data on wave response. Had larger waves been able to be generated, the initial force needed to displace the buoy would have been met, providing data with wave response. In order to obtain this data, a second experiment was devised.

The second experiment utilized a simplified model of the prototype in order to measure the generated wave characteristics. This model consisted of a foam tackle for the buoy, rubber bands of various thicknesses to act as a spring, and 50g weights to act as the mooring. A picture of the experimental set-up can be seen below in Figure 3.4.4.
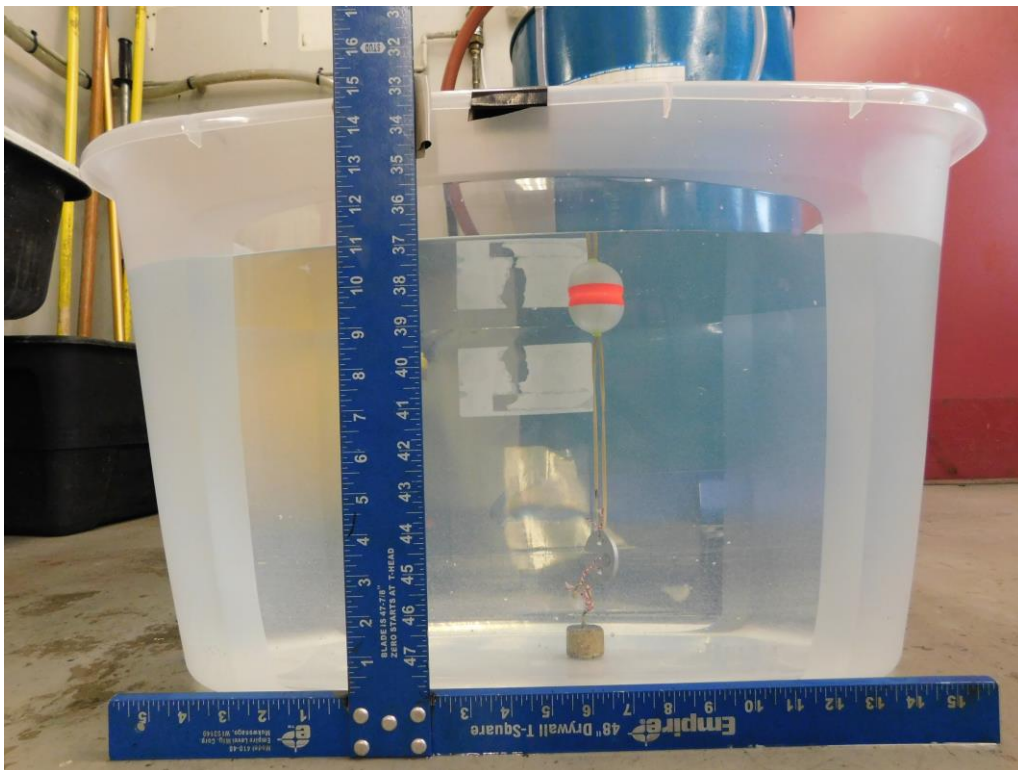

Figure 3.4.4 Wave Characteristics Experimental Set-Up

The spring constant of the rubber bands was determined by measuring the length of the unstretched rubber band and then hanging a weight from the rubber band and measuring the stretched length. By calculating the change in length and force applied, the spring constant for the rubber band was found by using Equation 3.4.1, where F is equal to the force, k is equal to the spring constant, and x is equal to the change in length. Full calculations and results can be seen in Appendix B.

$$F = -kx$$
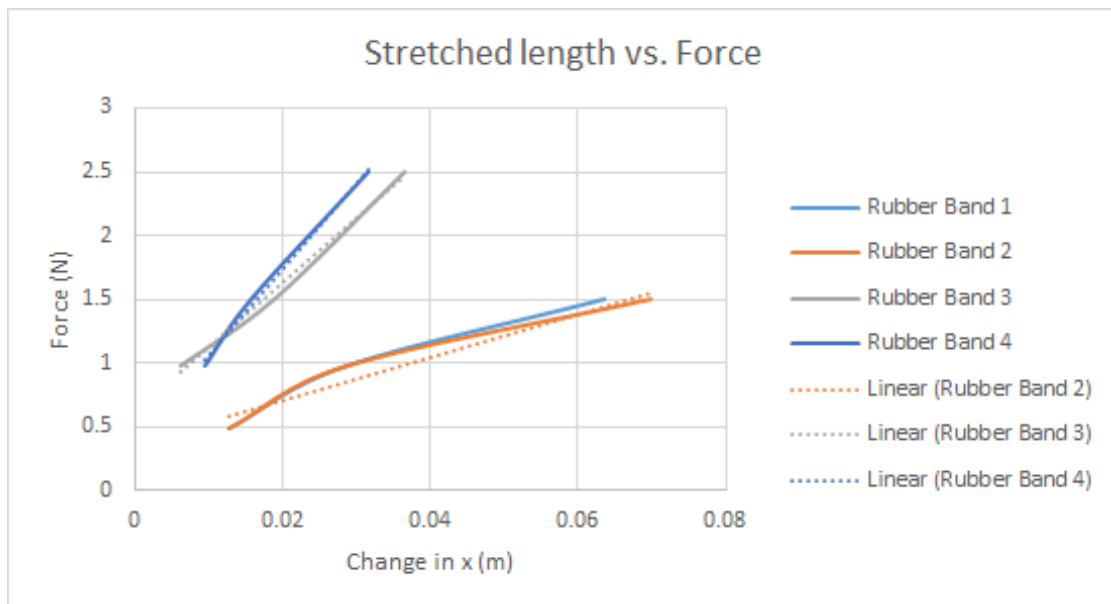
Equation 3.4.1: Spring constant

Figure 3.4.5 Force vs. position data for rubber bands used to calculate spring constant

Once the device was assembled, it was placed in a 30-gallon container of water and waves were generated through the oscillation of a curved piece of PVC. The device's response was recorded on a Nikon Coolpix B500 and the subsequent footage was uploaded to Tracker software where the motion of the tackle was tracked and graphed over time (Version 5.0.1, 2018). Additionally, the motion of the weight was tracked and subtracted from the position of the buoy to determine overall change in length of the rubber band. The y displacement of the buoy was subtracted from the initial position to determine the wave height.

These experiments provided a view into the power output of our prototypes, however there were many limitations. Neither experiment was able to be conducted with consistent waves, causing some gaps in data. This could have been addressed through the utilization of a wave tank

if the resource was available. Without the consistency, properties were still able to be empirically determined and results were obtained.

To determine how the data collected from each experiment could be related to the performance of a full scale WEC, a scaling factor was necessary. When scaling data from a prototype to a full-scale model, it is necessary to account for scaling effects to achieve similarity with the prototype. Scale effects are due to the fact that the force ratios are not identical between the model and its prototype, and this must be taken in consideration when analyzing the calculations for the full-size WEC. To scale from the experimental model to a full-scale WEC, Froude number similarity was used since most free surface flows are modeled after Froude (Heller, 2012).

The Froude scaling factor λ can be derived by equating the Froude number, F, for the full-scale model and the prototype:

$$F_F = \frac{V_F}{\sqrt{g_F L_F}} = \frac{V_P}{\sqrt{g_P L_P}} = F_P$$

Equation 3.4.2: Froude Similarity between Full Scale Model and Prototype

In the equation above, V corresponds to the velocity of the wave, g is the gravitational acceleration, and L is the characteristic length. Since the gravitational acceleration for the model and the prototype are the same, $g_F = g_P = g$. The characteristic lengths for the prototype and model can also be substituted into the equation above through geometrical similarity.

$$\lambda = \frac{L_F}{L_P}$$

Equation 3.4.3: Geometric similarity

Using geometric similarity to substitute $L_P = \lambda L_F$ into Equation 3.4.2, the following relationship between the wave velocities of the full-scale model and prototype can be derived. As shown below, a scaling ratio of $\lambda^{1/2}$ is needed to upscale Froude model velocities.

$$V_F = \lambda^{1/2} V_P$$

Equation 3.4.4: Froude scaling for wave velocities

Through a similar derivation process, the scale ratios associated with various parameters for Froude modeling were compiled into Table 3.4.1 below (Heller, 2012).

Parameter	Dimension	Froude Scaling Ratio
Length	$[L]$	λ
Area	$[L^2]$	λ^2
Volume	$[L^3]$	λ^3
Time	$[T]$	$\lambda^{1/2}$
Velocity	$[LT{-1}]$	$\lambda^{1/2}$
Acceleration	$[LT{-2}]$	1
Mass	$[M]$	λ^3
Force	$[MLT{-2}]$	λ^3
Pressure and Stress	$[ML{-1}T{-2}]$	λ
Energy and Work	$[ML^2T{-2}]$	λ^4
Power	$[ML^2T{-3}]$	$\lambda^{7/2}$

Table 3.4.1 Froude scaling ratio

4. Results and Analysis

4.1 Point Absorber Prototype

A revised testing procedure was conducted to measure the pressure change associated with piston movement. To begin, we placed the point absorber near the edge of the pool. In the initial testing period, wave generation in the pool was a major limitation. The layout of the pool consisted of drains located around the outer edge. These drains were slightly below water level to allow for water filtration, and any waves that were generated by the human subject would be lost in the drains. Without having a solid pool wall to push waves back and generate more momentum, the generated waves were too small to move the float on the prototype and generate displacement of the piston. As a result, the piston was manually displaced to its maximum stroke length of 6 inches by pulling the prototype down into the water and allowing the buoyancy force to extend the piston. When scaled up, the actual stroke length would be 7.5 ft.
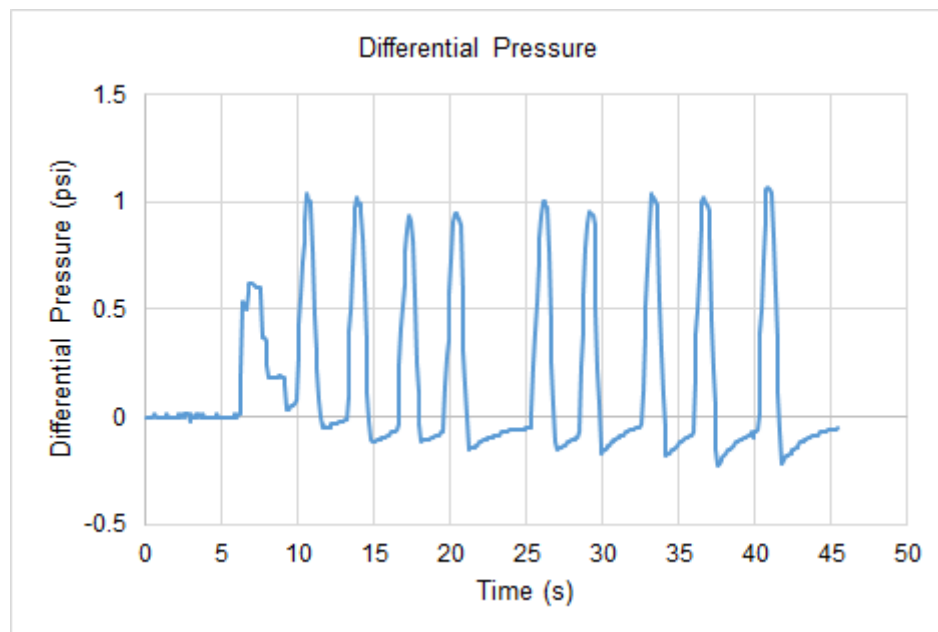

Figure 4.1.1 Differential Pressure measured at maximum stroke length

When collecting data from the differential pressure sensor, voltage measurements were collected which were then converted to differential pressure based off of the given hardware specifications of the sensor. This graph depicts the pressure change while the piston is displaced to its maximum stroke length over multiple iterations. By observing the data collected, it is apparent that the sensor reports a relatively consistent pressure difference over each stroke. The

22

magnitude pressure difference was found to be 1.066 psi. For this experimental run, the average time for one full stroke motion was 1.7 seconds.

In order to calculate the work done by the piston, Equation 4.1.1 was used where W is the work done by the piston, P is the pressure change, and V is the change in volume of the system. Knowing the vertical displacement of the piston, the change in volume was calculated to be 17.18 in^3. With the pressure change and volume change, the work of the piston was calculated to be 2.07 Joules. The work performed by the piston can also be equated to the energy that could produced by the prototype for each stroke.

$$W = PV$$

Equation 4.1.1: Work done by the piston

$$W = (1.066\ psi) * (17.18\ in^2) = (18.31\ lb\ in)\ * (\frac{0.1129\ J}{1\ in\ lb}) = 2.07\ J$$

In order to calculate the work output of the full-scale WEC, the corresponding Froude scaling ratio of λ^4 was used to upscale the work output calculated for the prototype. Considering that the prototype was designed to be a 1:15 scale model, $\lambda = 15$. Therefore, the estimated work output of a full scale WEC would be approximately 104.8 kJ per maximum stroke. The estimated time for the full-scale WEC to complete one full stroke can also be calculated using a Froude scaling ratio of $\lambda^{1/2}$, which was calculated to be 6.6 seconds. It is important to note that these calculations are assuming a 100% conversion efficiency of the system, whereas the actual efficiency of the system would be approximately 30-45% due to power generation losses in the PTO system and other losses such as distribution and transmission losses.

$$\lambda = 15$$
$$W_F = \lambda^4 W_P = (15^4) * (2.07\ J) = 104.8\ kJ$$
$$T_F = \lambda^{1/2} T_P = (15^{1/2}) * (1.7\ s) = 6.6\ seconds$$

4.2 Wave Characteristic testing

To understand the waves better, measurements were collected on rubber band displacement and wave height. From these measurements, the force was calculated with Equation 4.1.1. In this equation, F represents the force in newtons, k represents the spring constant of the rubber band in kg/s^2 (calculated in Appendix B), and Δx represents the change in length of the rubber band in meters.

23

$$F = -k\Delta x$$

Equation 4.1.1: Force of buoy

Our testing setup included a fishing tackle as the float, a rubber band as the spring, and a weight as a mooring system. The float was anchored to the bottom of the tub with an additional weight to limit movement in the X and Z directions. To manually create consistent waves, a curved section of PVC pipe was used. A camera was set up in front of the testing apparatus to record the wave and buoy motion for approximately 10 seconds. The video footage was imported into the Tracker software, which was used to manually track the displacement of the buoy, wave height, and weight position.

This testing did not take into account the strain of the rubber band, which is not negligible in rubber. Additionally, there were several unknown variables when testing. The waves could not easily be controlled, resulting in interference from waves rebounding off the sides of the tank. This caused a large variation of lag and lead time between the maximum wave and buoy height and t. The system was not constrained to Y motion, allowing displacement in the X and Z directions that normally a laboratory test would have designed against. The force could not be measured and was instead theoretically calculated. If this experiment were to be repeated, there are a number of recommended changes for successful data collection. The unknown variables need to be limited in order to have meaningful data.

5. Conclusions and Recommendations

It is important when considering the results of this project to also understand the limitations of wave energy harvesting. While waves are consistent and always available, too harsh of a wave can damage a system and too small of a wave will result in no movement of the piston. Waves are inherently unpredictable, so it is impossible to design a perfect system for harvesting their energy. Typically, wave energy conversion results in little power output because the floatation force can only counteract so much before the force of the wave takes over and the piston is fully extended. A buoy would have to be smaller than the height of a wave to ensure movement of the piston and prevent riding on top of a wave.

If this project were to be repeated, an enclosed and well controlled water environment is recommended. Ideally, this would be a wave tank in order to have consistent and controllable wave heights and periods. This would greatly benefit any scaling models, as most calculations rely heavily on the height of the wave.

For wave characteristic testing, constraining the buoy in only vertical motion would cause more ideal movement. A suggestion for this is mounting the system on a rail. Two air bearings could be used for an experiment of this size. To address the inconsistency in waves, a wave tank could be used to create controlled, consistent waves with no destructive interference. To compare force to the theoretical, force measurements should be taken during data collection. This could be done with a force transducer. Considerations for water-proofing the testing apparatus should also be made. This line of testing would be able to measure the force generated at different stiffnesses to determine a relationship between force exerted and stiffness of the system. It would also help determine an ideal stiffness of the system in order to obtain the the highest work output. A schematic of the suggested experimental setup can be seen in Figure 5.1, where 1 is the tank, 2 is the stationary slider which holds the float in place for testing, 3 is the float, 4 is the rubber band, and 5 is the weight.
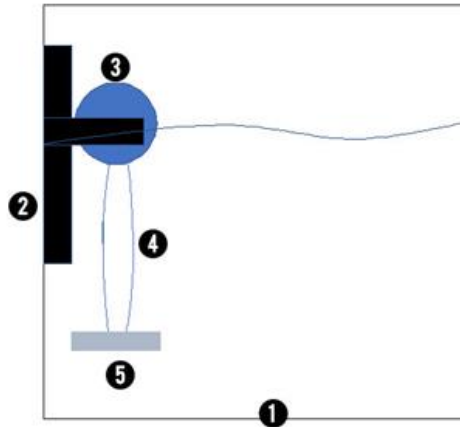
Figure 5.1 Wave Characteristic Experimental Setup

For future iterations of this project, we would recommend focusing on the optimal size of the float in comparison to the stiffness of piston. This would determine the best ratio for optimal energy harvesting. A piston with a low stiff response would result in a smaller force, limiting power generation. A piston with a high stiff response would result in limited movement and therefore also limit power generation. Finding the optimal stiffness would greatly benefit the field of ocean energy harvesting. This stiffness does change in relation to buoy size, so determining the shape of correlation would also be necessary. With a change in shape, it is also important to perform wave characteristic testing in order to determine how the buoy shape moves in conjunction with wave motion to prevent the overall system from being out of phase. We would recommend testing different spring stiffnesses with different float sizes to accomplish this experiment. Additionally, simulations of different buoy geometries would yield more insight into the system's response to waves and hence ability to harvest energy.

References

Amir, M. A. U., Sharip, R. M., Muzanni, M. A., & Anuar, H. A. (2016). Wave energy converters (WEC): A review of the technology and power generation. *AIP Conference Proceedings, 1775*(1) doi:10.1063/1.4965220

Autonomous underwater vehicles. Retrieved from http://www.whoi.edu/main/auvs Energy smart. Retrieved from http://www.whitehorse.vic.gov.au/IgnitionSuite/uploads/docs/Sustainable%20Living%20Guide%20Energy.pdf

Ewachiw, M. A., Jr. (2014). *Design of an autonomous underwater vehicle (AUV) charging system for underway, underwater recharging.* ().

Bergman, J. (2011). Temperature of ocean water. Retrieved from https://www.windows2universe.org/earth/Water/temp.html

Brown, D. (2018). Tracker (Version 5.0.1) [Computer software]. Retrieved from https://physlets.org/tracker/

BU-407: Charging nickel-cadmium. Retrieved from http://batteryuniversity.com/learn/article/charging_nickel_based_batteries

Chen, H., Cong, T. N., Yang, W., Tan, C., Li, Y., & Ding, Y. (2009). Progress in electrical energy storage system: A critical review. *Progress in Natural Science, 19*(3), 291-312. doi:10.1016/j.pnsc.2008.07.014

du Plessis, J. (2012). *A hydraulic wave energy converter.* ().

Duggan, W. (2016). wave power: The alternative energy dark horse. Retrieved from https://money.usnews.com/investing/articles/2016-12-06/wave-power-the-alternative-energy-dark-horse

Electricity in the United States. (2017, May 10). Retrieved April 16, 2018, from https://www.eia.gov/energyexplained/index.cfm?page=electricity_in_the_united_states

Engin, C. D., & Yeşildirek, A. (November 2015). Designing and modeling of a point absorber wave energy converter with hydraulic power take-off unit. Paper presented at the 1-6. doi:10.1109/EPECS.2015.7368507

Gaspar, J. F., Calvário, M., Kamarlouei, M., & Guedes Soares, C. (2016). Power take-off concept for wave energy converters based on oil-hydraulic transformer units. *Renewable Energy, 86*(Supplement C), 1232-1246. doi:10.1016/j.renene.2015.09.035

Heller, V. (2012). Model-prototype similarity. Retrieved from
http://www.drvalentinheller.com/Dr%20Valentin%20Heller_files/Heller_Model-
Prototype%20Similarity.pdf

Hong, Y., Waters, R., Boström, C., Eriksson, M., Engström, J., & Leijon, M. (2014). Review
on electrical control strategies for wave energy converting systems. *Renewable and
Sustainable Energy Reviews, 31*(Supplement C), 329-342. doi:10.1016/j.rser.2013.11.053

Nader, J. P., Dr. (2013). Interaction of ocean waves with oscillating water column wave energy
converters (Master's thesis, University of Wollongong, 2013). University of Wollongong.

Kongsberg.Autonomous underwater vehicle, REMUS 600. Retrieved from
https://www.km.kongsberg.com/ks/web/nokbg0240.nsf/AllWeb/F0437252E45256BDC12574
AD004BDD4A?OpenDocument

Ocean Power Technologies. (2011). Company presentation Ocean Power Technologies.
Retrieved from https://oceanpowertechnologies.gcs-web.com/static-files/212d7a27-1fee-40cc-
92e2-ca600045c8a0

Ocean Power Technologies. (2017). Ocean power technologies: In the news. Retrieved from
http://www.oceanpowertechnologies.com/resources/

Ocean wave energy. Retrieved from https://www.boem.gov/Ocean-Wave-Energy/

Poullikkas, Andreas. (2014). Technology prospects of wave power systems. Electronic Journal
of Energy & Environment.

Raghunathan, V., Kansal, A., Hsu, J., Friedman, J. K., & Srivastava, M. B. (2005). Design
considerations for solar energy harvesting wireless embedded systems
. *Eastern-European Journal of Enterprise Technologies, 2*(12(68)), 72. doi:10.15587/1729-
4061.2014.23865

Simple and robust construction - complex design   (2005). Retrieved from
http://www.wavedragon.net/index.php?option=com_content&task=view&id=6

Têtu, A. (2017). *Power take-off systems for WECs* Springer, Cham. doi:10.1007/978-3-319-
39889-1_8

Ulvin, J. B., Molinas, M., & Sjolte, J. (2012). Analysis of the power extraction capability for
the wave energy converter BOLT®. *Energy Procedia, 20*(Supplement C), 156-169.
doi:10.1016/j.egypro.2012.03.017

U. (2017). Attenuator (Pelamis - Pelamis Wave Power). Retrieved April 1, 2018, from
http://www.esru.strath.ac.uk/EandE/Web_sites/14-15/Wave_Energy/attenuator.html

Voorhis, R. (2012, July 25). Point Absorbers: The Technology and Innovations. Retrieved April 24, 2018, from http://coastalenergyandenvironment.web.unc.edu/ocean-energy-generating-technologies/wave-energy/point-absorbers/

Wang, L., & Isberg, J. (2015). Nonlinear passive control of a wave energy converter subject to constraints in irregular waves. *Energies, 8*(7), 6528-6542. doi:10.3390/en8076528

Wave Energy. (n.d.). Retrieved from http://www.oceanenergycouncil.com/ocean-energy/wave-energy/

4 Charts That Show Renewable Energy is on the Rise in America. (2016, November 14). Retrieved April 16, 2018, from https://www.energy.gov/eere/articles/4-charts-show-renewable-energy-rise-america

Appendix A: Prototype Parts

Major Components

Buoy

19.90 oz.

8" diameter

Copper

Pneumatic Cylinder

2-1/2" Air Cylinder Bore Dia with 6" Stroke

Stainless Steel

Nose Mounted Air Cylinder

Polycarbonate Tube

3-1/2 inch outside diameter x 4 ft. long

<u>Heave Plate</u>
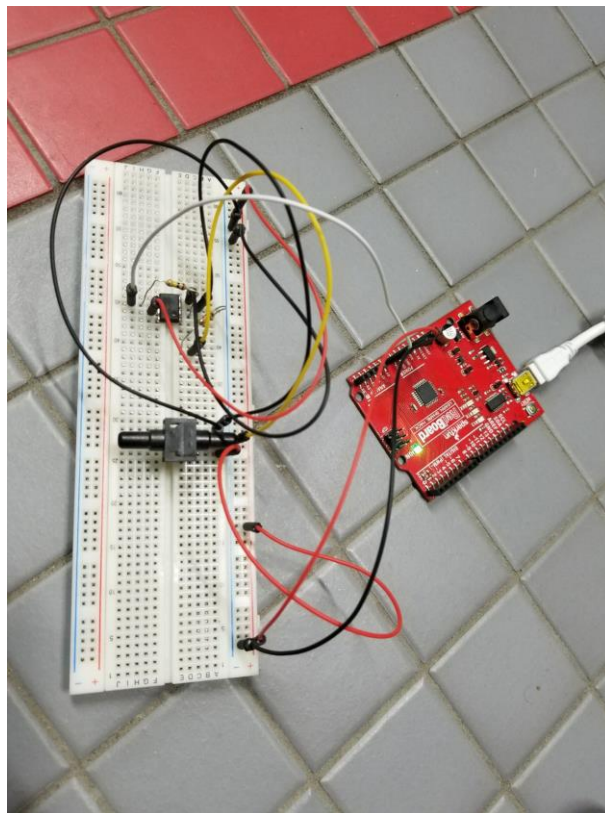
Acrylic Plate

½ inch thick
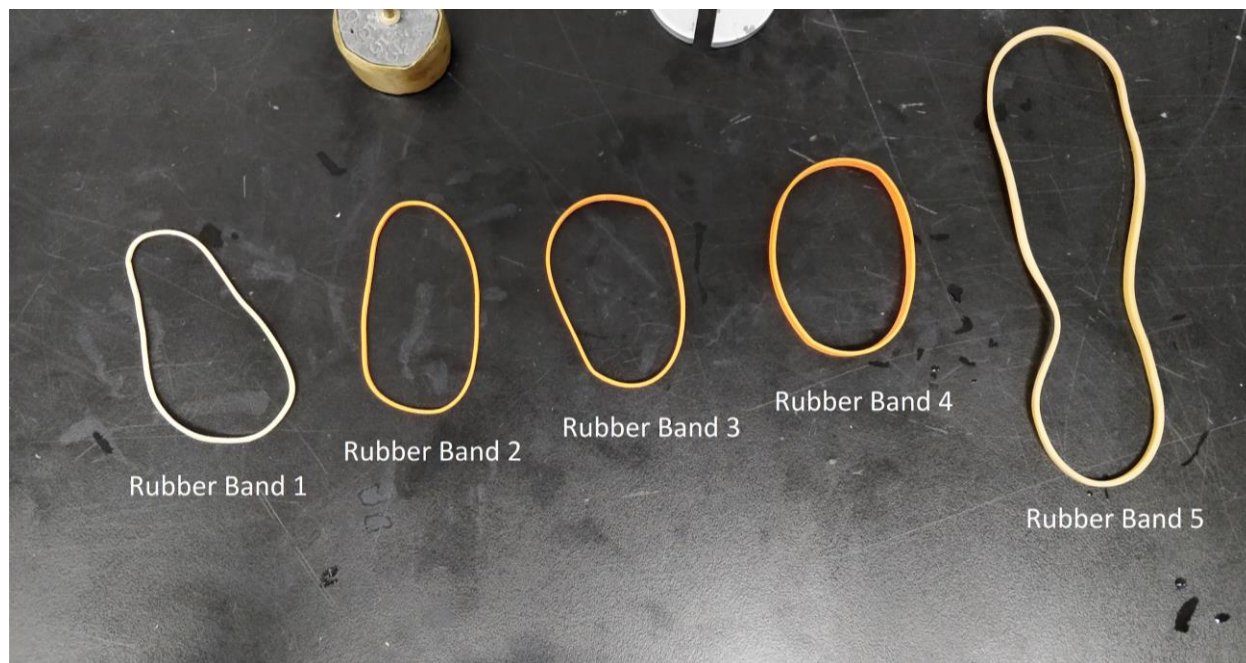

Smaller Components

-   Wing nut ¼ in - 20
-   Hose clamp
-   Dual flush repair kit - rubber gasket
-   Zinc plated screw eyes #210
-   Loctite marine adhesive sealant
-   Acrylic Cement
-   Zinc plated chain
-   Hose barb adapter ⅜ ID x ¼ in MIP

Electronics

- Duracell 9 V batteries
- Arduino Kit
- Breadboard
- Differential gage pressure sensor

-

Appendix B: Spring Constants of Rubber Bands

Rubber Band (initial length)	Weight (g)	Δx (in)	k (kg/s^2)
1 (3.5 in)	50.02	0.5	39
	100.01	1.125	34
	153.6	2.5	24
2 (3.25 in)	50.02	0.5	39
	100.01	1.125	34
	153.6	2.75	22
3 (3.25 in)	100.01	0.25	155
	153.6	0.75	79
	254.72	1.4375	68
4 (7.125 in)	100.01	0.375	103
	153.6	0.625	95
	254.72	1.25	79

Sample Calculation:

Rubber band 1:

$$F = -kx$$

$$F = ma = (50.02g)(-9.81m/s^2)(\frac{1\,kg}{1000\,g})$$

$$F = -0.49\,N$$

$$-0.49\,N = -k(0.5\,in)(\frac{2.54\,cm}{1\,in})(\frac{1\,m}{100\,cm})$$

$$k = 39\,kg/s^2$$